



Quasi-static Cyclic In-plane Testing of Slender GFRP-Reinforced Concrete Shear Walls

Hany el-Kady¹, Osama Amer², Ashraf Shawky³, Ahmed H. Ali¹, Hesham Haggag¹

¹Department of Civil Engineering Helwan University, Cairo, Egypt

²Department of Civil Engineering, Ain Shams University, Cairo, Egypt

³Department of Civil Engineering, Cairo University, Cairo, Egypt

Keywords

*Hysteretic behaviour,
Reinforced concrete,
Shear walls,
Equivalent viscous damping,
Seismic Performance,
Cyclic load*

Abstract

Using Glass fiber-reinforced polymer (GFRP) bars as a replacement for conventional steel bars is one of the most potential solutions to steel-corrosion-related problems in concrete. Their durability and high strength-to-weight ratio make them a cost-effective and applicable alternative to conventional steel bars. This study investigates the characteristic behavior of concrete shear walls reinforced with steel, GFRP, and a hybrid scheme of steel and GFRP bars under seismic loading. Six full-scale RC shear walls with an aspect ratio of 3.25 were tested under pseudo-static reversed-cyclic lateral load to investigate the potential of a hybrid reinforcement scheme of steel-GFRP to improve the seismic behavior of slender RC shear walls. The overall performance of each tested wall was characterized by investigating the hysteretic response, crack propagation, lateral load capacity, and energy dissipation behavior.

Furthermore, the effects of the GFRP web reinforcement ratio on different behavioral aspects are also investigated. The results indicated that the GFRP-reinforced concrete cantilever walls had an elastic behavior with recoverable deformation up to more than 80% of its ultimate lateral strength. A considerable enhancement in the self-centering capacity of hybrid GFRP-steel reinforced walls was observed, which helped to mitigate the experienced concrete damage. Moreover, higher displacement capacity, increased lateral strength, and equivalent viscous damping coefficient were attained with the GFRP web reinforcement ratio.

1. Introduction

The use of reinforced concrete (RC) walls is frequently recommended as a reliable bracing solution with promising performance for lateral load resistance and drift control in mid and high-rise buildings. This fact was experimentally confirmed in literature as Reinforced Concrete (RC) shear walls offered high lateral strength, stiffness, and deformation capacity under seismic loading. Therefore, it is essential to understand the actual behavior of RC shear walls and their seismic performance. Extensive investigations are also essential to analyze their failure mechanisms appropriately and create more dependable and cost-effective designs, especially since performance-based design techniques are increasingly frequently used for new structures [1-3].

A shear strength failure criterion for shear walls was established in earlier investigations [4]. In the study, a database of the previous testing on minimally reinforced shear walls was put together and examined. The findings showed that the quantity of boundary reinforcement provided, the existence of axial load, and the position of a weak plane joint on the wall were the most significant elements that affect the nominal shear strength. Oh et al. [5] studied the effect of boundary element details, confinement, and end configurations of RC structural walls on their deformation capacities. The study included testing Four full-scale wall specimens (three rectangular and a barbell-shaped cross-section wall) having different transverse reinforcement content at the boundaries. The authors concluded that the barbell and the well-confined rectangular wall showed similar deformation capacities, drift ratios, and energy dissipation. Beyer et al. [2], tested half-scaled U-Shaped/ channel-shaped structural walls to evaluate their flexural behavior in different loading directions. The tests indicated that the most critical direction was the diagonal

loading direction, where the displacement capacity was the smallest. Preti and Giuriani [6] investigated the ductility of the reinforced concrete structural walls in buildings of mid-rise height. In this study, a full-scale five-story RC wall was tested. The wall was reinforced with unusually large rebar diameters uniformly distributed along the wall length. High ductility capacity was attained for the tested wall, ensuring a uniform crack pattern and eliminating any premature web rebar fracture, shear sliding, and crack localization in the web region.

According to experimental findings in the literature, the behavior of shear walls is primarily depended on the geometric characteristics of the walls; for squat walls ($\alpha_s = h_w/l_w \leq 2$), the response is governed by shear, while the response of slender walls ($\alpha_s \geq 2$) is dominated by flexural [1,4,7]. This study focuses on slender shear walls, commonly used for mid- and high-rise buildings. They are usually designed to resist lateral loads primarily through flexural behavior and to withstand significant inelastic flexural deformations prior to strength loss, i.e., ductile behavior.

The selection of reinforcement is one of the most crucial factors to be considered when designing reinforced concrete (RC) structures. Although conventional steel has long been the most common reinforcement for concrete structures, its susceptibility to corrosion presents a significant problem for buildings in harsh climates. Steel corrosion causes the effective cross-section of the reinforcing bars to decrease drastically, eventually resulting in unexpected failures. Corrosion causes a reinforcing steel bar's volume to increase by up to three times its initial size. Additionally, the surrounding concrete might also spall and crack as a result of that expansion [3]. Conversely, GFRP reinforcing bars are inherently immune to corrosion, which offers a desirable alternative to conventional steel reinforcement for

*Corresponding Author: osama_amer@cu.edu.eg

Received 21 October 2022; Revised 25 October 2022; Accepted 25 October 2022

2687-5756 /© 2022 The Authors, Published by ACA Publishing; a trademark of ACADEMY Ltd. All rights reserved.

<https://doi.org/10.36937/cebel.2022.1737>

reinforced concrete structures, including columns, beams, and one-way and two-way slabs [8-13].

The interest in using Glass fiber reinforced polymer (GFRP) bars lies within their resistance to corrosion of the reinforced concrete structures where climatic condition is aggressive [14,15]. Besides high corrosion resistance, GFRP bars in reinforced concrete structures have shown advantages such as a higher tensile strength-to-weight ratio than steel reinforcement and their ability to conform to uneven surfaces. Seven low-rise squat walls, with an aspect ratio (α_s) of 0.8, were tested with carbon FRP (CFRP) grids by Yamakawa and Fujisaki [16]. The authors indicated that significant self-centering performance was attained as a result of the CFRP material's linear elastic response. However, an early fracture of the CFRP grids occurred, which led to low ductility and decreased energy dissipation capacity. The increased self-centering performance and limited energy dissipation capacity were also confirmed through the study conducted by Mohamed et al. [17]. The study included three GFRP-reinforced shear walls with different aspect ratios tested under in-plane cyclic loading.

Moreover, Mohamed et al. [17] conducted experimental research on GFRP-reinforced shear walls subjected to lateral cyclic loading. According to the results, adequately designed and detailed GFRP-reinforced shear walls can reach their flexural strengths without experiencing significant degradation. Arafa et al. [18] also concluded, through their experimental study on GFRP-reinforced shear walls, that higher deformation capacity can also be achieved if the walls were adequately detailed and sufficient shear reinforcement was adopted. Additionally, more effective confinement and ductility can be attained by using closely spaced GFRP transverse reinforcement [19]. According to Zang et al. [20], the same deformation ability and load-carrying capacity of RC shear walls could be attained by GFRP reinforcement compared to the same reinforcement ratio of steel. More recently, Islam et al. [21] tested two GFRP-reinforced shear walls with different web horizontal reinforcements under in-plane quasi-static cyclic loading. The results indicated that the strength and drift capacity could be increased, and the crack widths could be reduced by increasing the horizontal web reinforcement.

Although the advantages of GFRP reinforcement are discussed above, there are still few applications of FRP, and its use is not widespread. Lack of design knowledge among practicing engineers is one of the primary challenges facing the designer of FRP-reinforced concrete elements. The nearly elastic stress-strain response of FRP reinforcing materials is another limitation since it precludes their application in areas prone to seismic events where ductility and nonlinear behavior are desired [3]. Thus, this research aims to determine whether GFRP bars could be used as a primary reinforcing element or as part of a hybrid GFRP-steel reinforcement for reinforced concrete shear walls. The study mainly focused on the performance of slender (flexural controlled) shear walls, as they are commonly used in mid-to high-rise buildings. The main objectives are to:

- a. Better understand the failure mechanisms of GFRP-RC shear walls by evaluating their behavior and response under in-plane cyclic loads.
- b. Evaluate the viability of GFRP-reinforced walls to achieve reasonable strength, flexural/shear capacity, and deformability requirements of drift and energy dissipation that are substantially required in the concrete lateral resisting system.
- c. Investigate the effect of using hybrid GFRP-steel reinforcement on the structural performance of shear walls compared to conventional steel-reinforced shear walls.

Although the current study considered only one type of FRP reinforcement, GFRP, the results can still be easily implemented in other FRP types.

2. Testing process

2.1. Wall Specimens

Six RC shear walls were tested as part of the experimental program under quasistatic cyclic loading till failure. The tested walls included three GFRP-reinforced specimens (GW1, GW2, and GW3), one reference steel-reinforced specimen (SW1), and two walls with hybrid GFRP-steel reinforcement (SGW1 and SGW2). The minimum thickness and reinforcement details were designed according to [22] for the steel-reinforced wall and [23] for the GFRP-reinforced walls. Plane sectional analysis was adopted to predict the ultimate lateral load (Figure 1), assuming the concrete compressive strain (ϵ_{cu}) limit equals 0.003. Internal force equilibrium (Eq. 1) and strain compatibility relationship (Eq. 2) formed the bases for the utilized plane-sectional analysis [24]; consequently, the flexural strength of the RC wall was determined.

$$M_i = C_c \left(c - \frac{a}{2} \right) + \sum_1^n A_{si} f_{si} (c - X_i) + P_i \left(\frac{l_w}{2} - c \right) \tag{Eq. 1}$$

$$\epsilon_{si} = \epsilon_{cu} \frac{c - X_i}{c} \tag{Eq. 2}$$

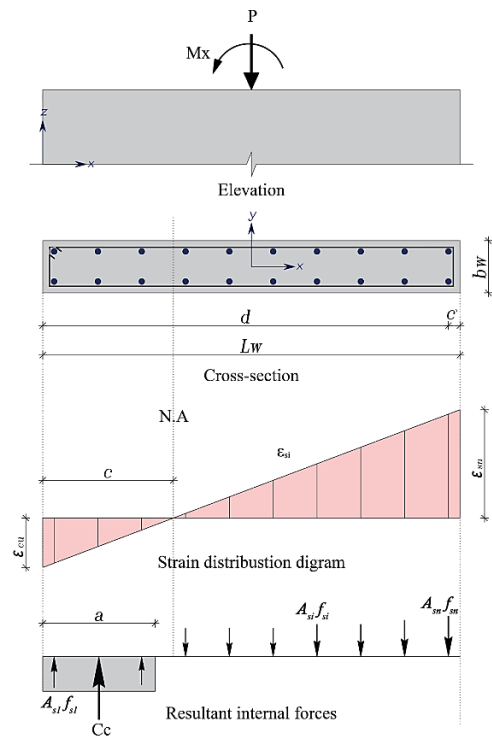


Figure 1 – Force equilibrium and strain distribution in wall cross-sections

The theoretical shear strength (V_r) was determined using sectional shear-analysis equations as the sum of the concrete shear strength (V_c) and the shear strength (V_f) provided by horizontal web reinforcement [25], as shown in Eq. 3-5.

$$V_r = V_c + V_f \tag{Eq. 3}$$

$$V_c = \frac{2}{5} \sqrt{f'_c} b_w (kd) \tag{Eq. 4}$$

$$V_f = \frac{A_{fv} f_{fv} d}{s} \tag{Eq. 5}$$

The tested walls were designed with adequate reinforcement to ensure flexural domination and prevent sliding shear and anchorage failures. Moreover, two layers of vertical reinforcements were provided for all walls to limit the potential out-of-plane displacement and increase the walls' stability [26,27], as shown in Table 1. Figure 2 presents the concrete dimension and reinforcement details of the tested walls.

2.2. Materials

All specimens were constructed using normal-weight and ready-mixed concrete with a targeted concrete compressive strength (f'_c) of 30 MPa. Three concrete cylinders with 150mm diameter and 300mm height were prepared from each pour and tested under compression following [28]. For steel reinforcement, 8mm Grade 240/350 steel bars

were used for horizontal reinforcement, and 12mm Grade 400/600 steel bars were used for vertical reinforcement. Moreover, #4 sand-coated straight GFRP reinforcing bars were used for the horizontal and vertical reinforcement ($f_{fu} = 1392MPa, E_f = 69.6GPa, \epsilon_{fu} = 2\%, A_f = 126.7 mm^2$). U-shaped steel bars of 8mm diameter were used at both ends of the GFRP-reinforced walls to avoid the bent proportion of GFRP bars (Figure 3).

2.3. Testing and instrumentation

A lateral reverse-cyclic load was applied at the top of the walls using a displacement-controlled hydraulic actuator with a maximum stroke of ± 250 mm while restraining any potential horizontal movement at the base and the vertical movement of each tested wall.

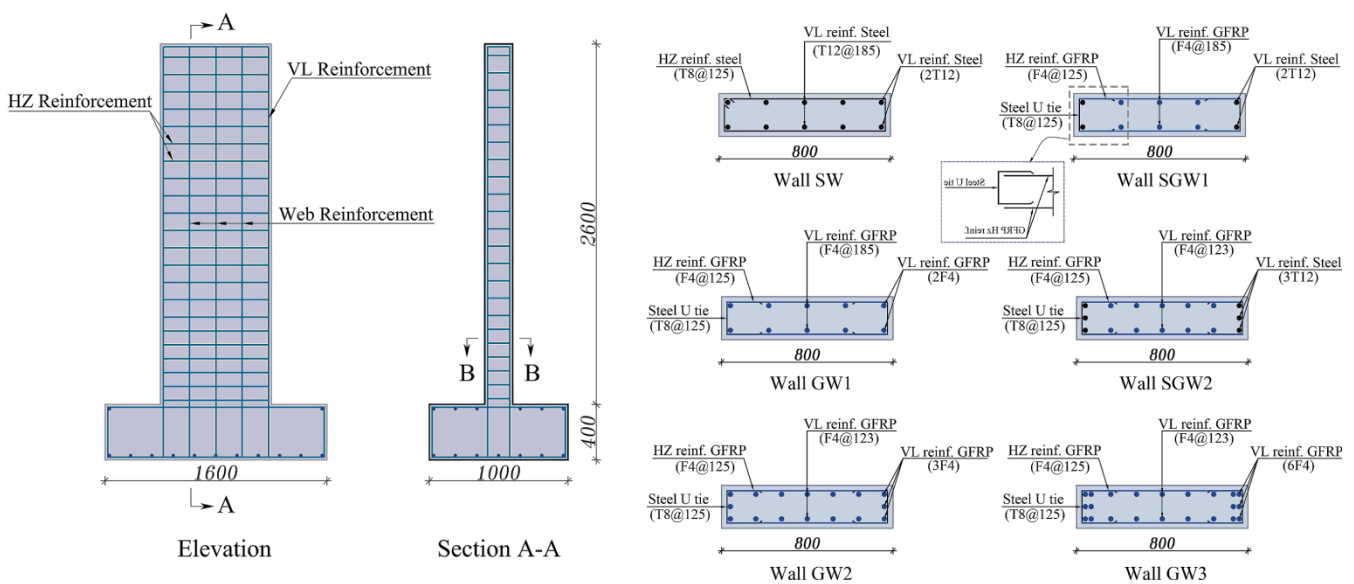


Figure 2 – Concrete dimensions and details of reinforcement configuration of walls (a) SW1 (b) SGW1, (c) GW1, (d) SGW2, (e) GW2, and (f) GW3. All dimensions in mm

Table 1 - Details of the wall specimens

Specimens	Vertical reinforcement (%)				Horizontal reinforcement			Predicted capacity (kN)
	No. & size	$\rho_{V,s}$	$\rho_{V,f}$	No. & size	$\rho_{h,s}$	$\rho_{h,f}$		
Steel-Reinforced wall	SW - Control	10 T12 ^a	0.71	-	T8 ^b @ 125 mm	0.40	-	86.00
Hybrid GFRP-steel reinforced walls	SGW1	4 T12 + 6F4 ^c	0.28	0.48	F3@ 125 mm	-	1.01	97.64
	SGW2	6 T12 + 10F4	0.42	0.79	F3@ 125 mm	-	1.01	93.17
GFRP-reinforced wall	GW1	10F4	-	0.79	F3@ 125 mm	-	1.01	133.83
	GW2	16F4	-	1.27	F3@ 125 mm	-	1.01	140.85
	GW3	22F4	-	1.74	F3@ 125 mm	-	1.01	174.75

^aSteel bars $d_b = 12mm$; ^bSteel bars $d_b = 8mm$; ^cGFRP bars No. 4.

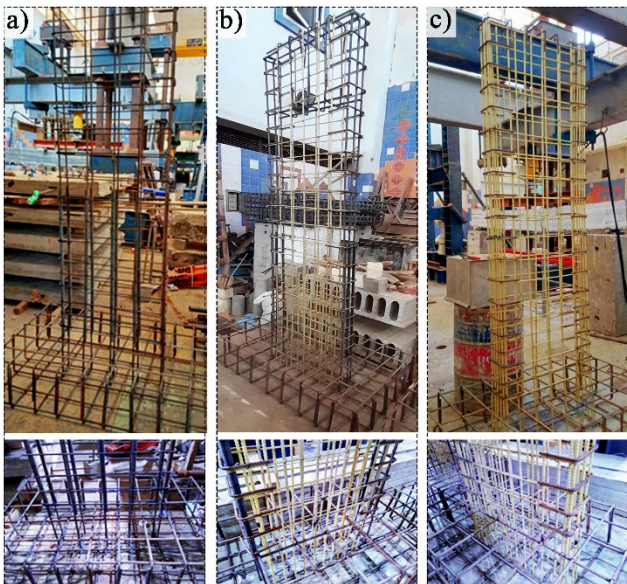


Figure 3 – Reinforcement configuration of (a) steel, (b) hybrid steel-GFRP, and (c) GFRP reinforced walls

No axial load (other than self-weight) was applied to walls during testing. Five LVDTs were used to measure and record the vertical and lateral displacements at various points. Strain gauges were attached to the two outermost vertical reinforcement bars 100 mm above the interface between the wall and the foundation.

The horizontal deflection was measured at the top of each wall to control the displacement protocol. The wall specimen was positioned between two reaction steel frames, and a specially fabricated load transfer system was fixed on the wall's top height, consisting of steel-plated and high-strength steel rods. The lateral load was applied at the steel girder using a 500 kN hydraulic actuator, which was fixed to the strong reaction frame and the load-transfer system of the walls, as shown in Figure 4. The imposed lateral loading protocol comprised two fully-reversed lateral drift cycles (Figure 4b) applied at gradually increasing drift levels as per FEMA 461-07 [29].

3. Main test results

3.1. Hysteretic displacement response

The shear wall's seismic performance significantly depends on the force versus displacement relationship. Continuous plots of applied

force versus displacement hysteresis relationships and envelope curves of all tested walls were recorded and plotted in Figures 5-7.

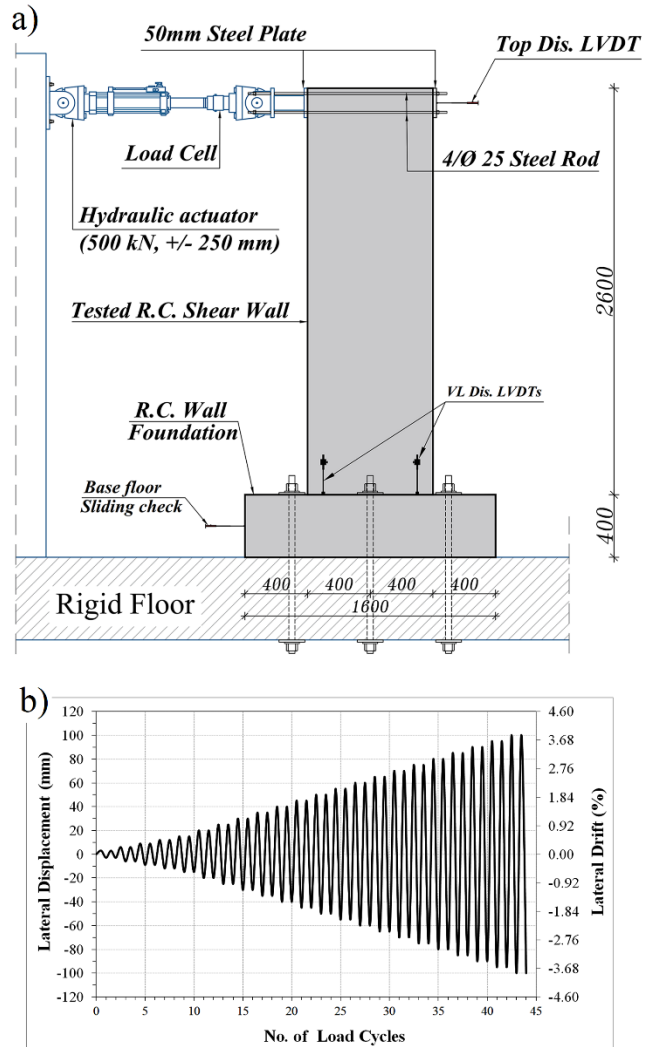


Figure 4 – Layout of the test setup and used LVDTs (a), and (b) Applied displacement-controlled loading history

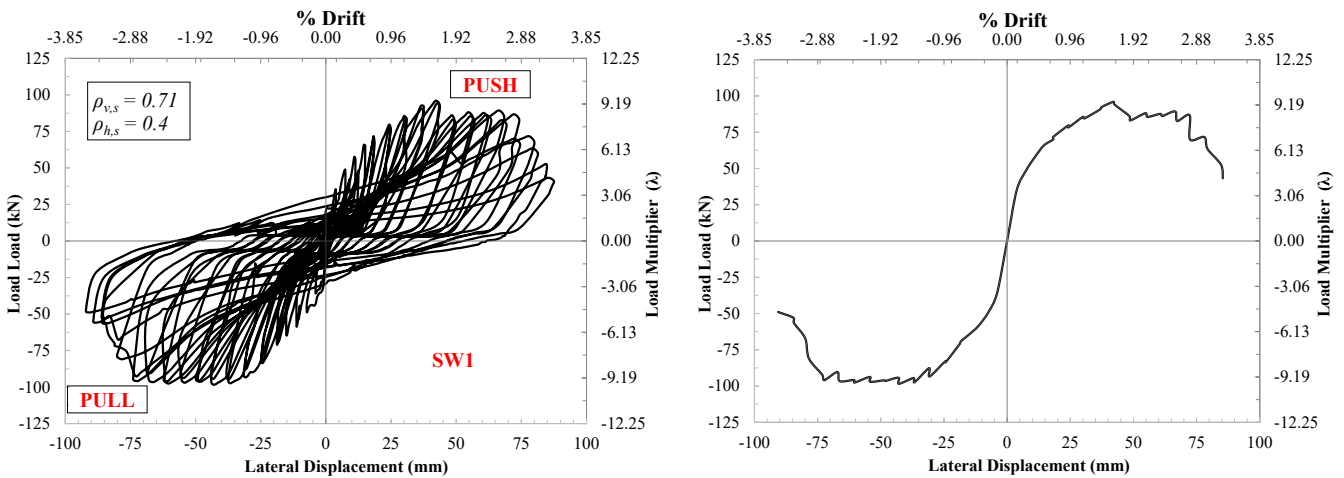


Figure 5 – Hysteretic load-displacement response and envelope curve of wall (SW1)

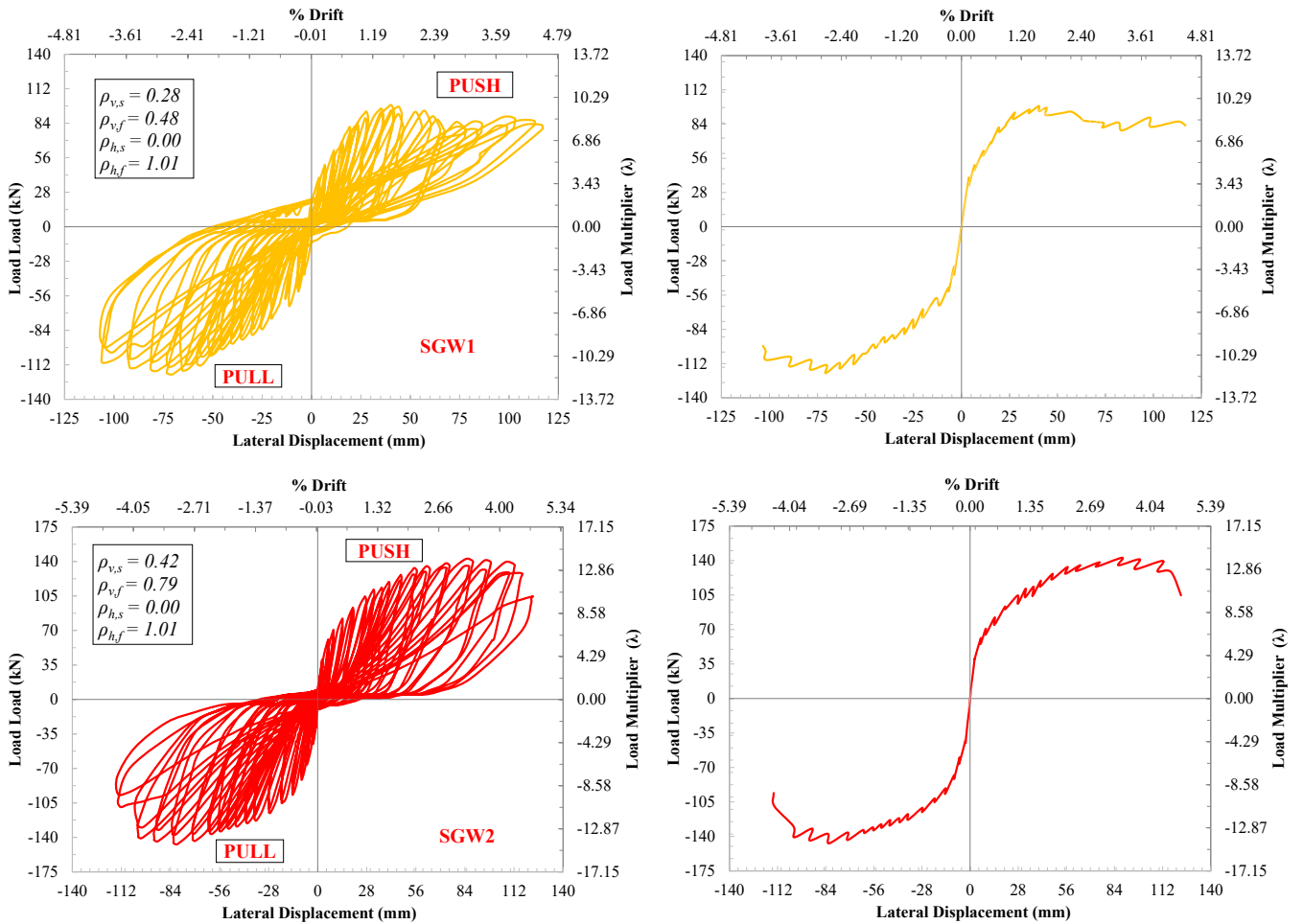


Figure 6 – Hysteretic load-displacement response and envelope curve of walls (SGW1 and SGW2)

In each graph, the vertical, ρ_v , and horizontal, ρ_h , reinforcement ratios are shown. The top right quadrant shows the load-displacement relationships in the push (+) direction, and vice versa for the bottom left quadrant, which plots the load-displacement relationships in the pull (-) direction.

The primary axes plot the lateral force (F) acting on the wall versus the top displacement (Δ) obtained from the recorded displacement from the top horizontal LVDT. The secondary axes of the presented graphs display the drift (δ) versus load multiplier (λ). The load multiplier (non-dimensional load format) is defined as the ratio of the wall's lateral force resistance to its self-weight $\lambda = \frac{Q}{W_w}$.

Overall, the hysteretic response of the tested walls appears to be self-centering and showed reasonably stable lateral load-displacement relationships. The behavior in the push and pull loading directions was almost symmetric, with no significant load or displacement residuals over a large part of the test until concrete crushing occurred at one end.

For steel-reinforced and hybrid steel-GFRP reinforced walls (SW and SGW), the performance of the specimens was initially elastic, followed by an inelastic behavior with gradual degradation in stiffness until the failure occurred. The hysteretic curves presented thin and slender loops upon the yielding of the outmost steel bars, indicating initially stiff behavior and a lower level of damage. The slope of the curve decreased in each loading cycle beyond the initial uncracked stage.

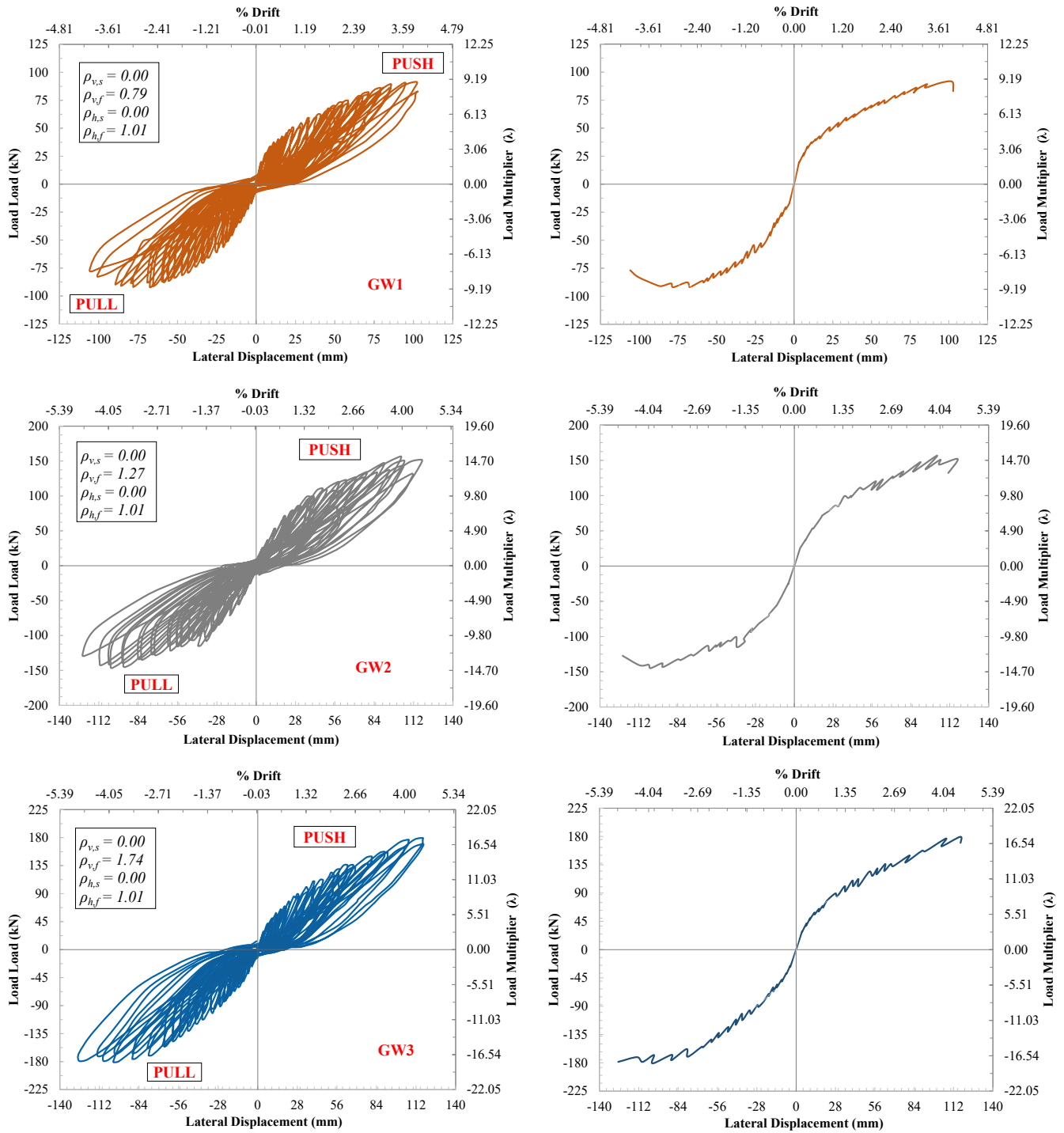


Figure 7 – Hysteretic load-displacement response and envelope curve of walls (GW1, GW2 and GW3)

With the subsequent cycling of the wall, the slope of the curve further degraded into relatively wider loops of higher displacement levels. Further opening of the loops indicates a higher damage level, which would increase energy dissipation capabilities. Contrarily, the GFRP reinforcement's elastic behavior and the lack of yielding led to a continuously increasing gain in strength up to failure, with no strength degradation within a reasonable range of deformations. The loading, unloading, and reloading curves demonstrated linear behavior with narrower hysteresis loops than the corresponding steel-reinforced walls following the elastic behavior of GFRP bars. The behavior was almost symmetric up to failure in both push and pull loading directions, resulting in a pinched hysteresis response without any reduction of overall strength. This stable hysteresis loop behavior is typical of a response that is flexural-dominated.

3.2. Failure modes and extent of damage

In general, the behavior of all walls was dominated by a flexural response. However, crack patterns differed during loading cycles due to different reinforcement types and ratios. The specimens exhibited nearly linear behaviour before cracking. Almost a similar strength level corresponding to the crack initiation was attained for all tested walls, as it mainly depends on the concrete compressive strength. The first horizontal flexural crack for all the tested walls was initiated at the bottom of all walls at an average drift level of 0.22%. Likewise, the concrete-cover splitting at the wall edge was recorded at almost similar drift levels ranging between 0.7% and 0.83%, where the concrete compressive strain exceeded 0.003. The cracks developed in succession from the bottom of the wall up to a height of approximately $(2/3)h_w$ and were accompanied by diagonal shear flexural cracking of the web without any premature shear or anchorage failure. The failure mode for all walls was characterized by horizontal cracking and concrete spalling, followed by the formation of flexural cracks at the base cross-section as a result of the growing bending moment. More significant spalling of the concrete cover at the compression end of the wall is attained with increasing displacement accompanied by buckling/rupture of the outermost vertical reinforcement bars and crushing of the concrete at the toes. The failure of steel-reinforced and hybrid steel-GFRP-RC walls followed a remarkably similar pattern, characterized by local buckling of outmost longitudinal steel bars and crushing of concrete at the toe of the walls.

However, hybrid specimens featured fewer residual drift ratios than the control wall (SW1). The GFRP-reinforced walls exhibited notable linear behavior up to its ultimate strength, where the failure stage started at the peak load and lasted until the test's end. Concrete cover splitting was gradually initiated at the outmost heavily compressed wall toe. As loading continued, the walls continued to carry the load in each cycle with no strength degradation until concrete crushing and fracture of the longitudinal GFRP bars occurred, which caused wall brittle failure without a considerable decrease in the recorded walls' strength. Further, higher GFRP-reinforcement ratios resulted in higher crack propagation and brittle failure. A combined shear-flexure failure mechanism was only observed in walls GW2 and GW3, where sliding shear deformations are developed after maximum strength due to the web's diagonal cracking. Figure 8 summarises all tested walls' recorded maximum displacement and ultimate load capacity. The performance parameters recorded at the primary damage levels are summarized in Figure 9. The final crack patterns and typical failure modes of the specimens are shown in Figure 10. Close-up photos of the major damage aspects are presented in Figure 11.

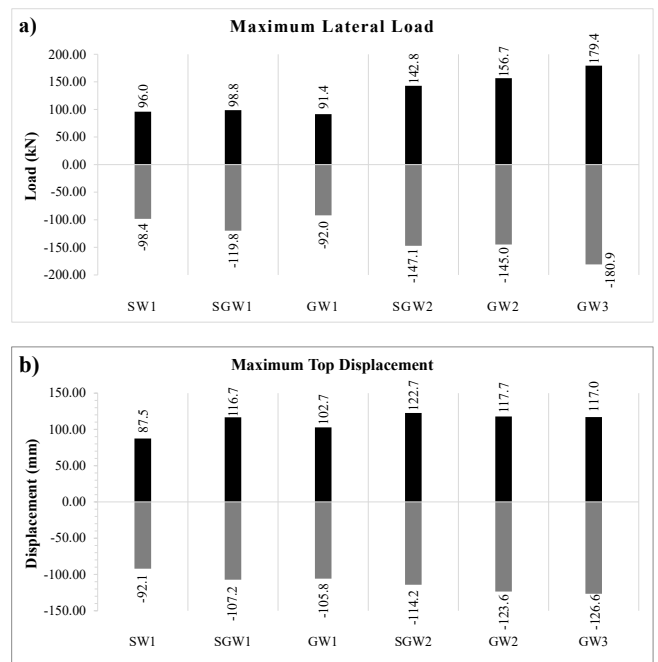


Figure 8 – Comparison between the maximum recorded loads (a) and displacement (b) of all tested walls

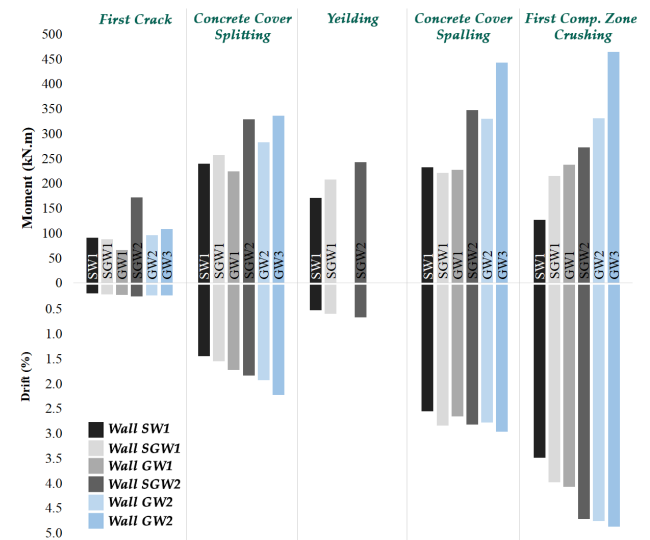


Figure 9 – Summary of damage propagation for all tested walls

4. Characteristic experimental behaviour

4.1. Overview of walls behavior

The hysteretic response of the GFRP-reinforced walls exhibited a reasonably stable lateral load-displacement relation displaying no strength degradation throughout a realistic range of deformations. The ultimate lateral strength of GFRP RC wall GW1 was found to be 6.4% lower than that of wall SW1. While wall SW1 attained its maximum strength at a displacement level of $0.46\Delta_{max}$, wall GW1 reached its maximum strength at a higher displacement level of $0.73\Delta_{max}$ at the maximum recorded load. Moreover, moderate damage occurred at higher drift levels for GFRP hybrid GFRP-steel reinforced walls. These results are in agreement with the literature [17,30] where the GFRP-reinforced walls exhibited elastic behavior, including realigned cracks and recoverable deformation up to higher drift levels.

It was confirmed by comparing walls GW2 and GW3 to wall GW1 that increasing the GFRP reinforcement ratios results in increased displacement as well as an increase in lateral load capacity. At higher drift levels, a softening behavior of GFRP-reinforced walls was exhibited with the propagation of cracks that closed and realigned after each cycle. Each wall maintained its lateral load capacity even after full cracking at increasing levels of displacement without strength decay, which is addressed by the linear elastic behavior of GFRP bars. This softening behavior of GFRP-reinforced walls is in agreement with the literature [17, 24].

For hybrid GFRP-steel reinforced walls, the lateral load resistance of wall SGW1 was similar to that of wall SW1. However, because of the linear elastic behavior of the incorporation of GFRP bars, a higher displacement level corresponding to the ultimate load capacity was achieved in wall SGW1 due to the elastic behavior of GFRP bars.

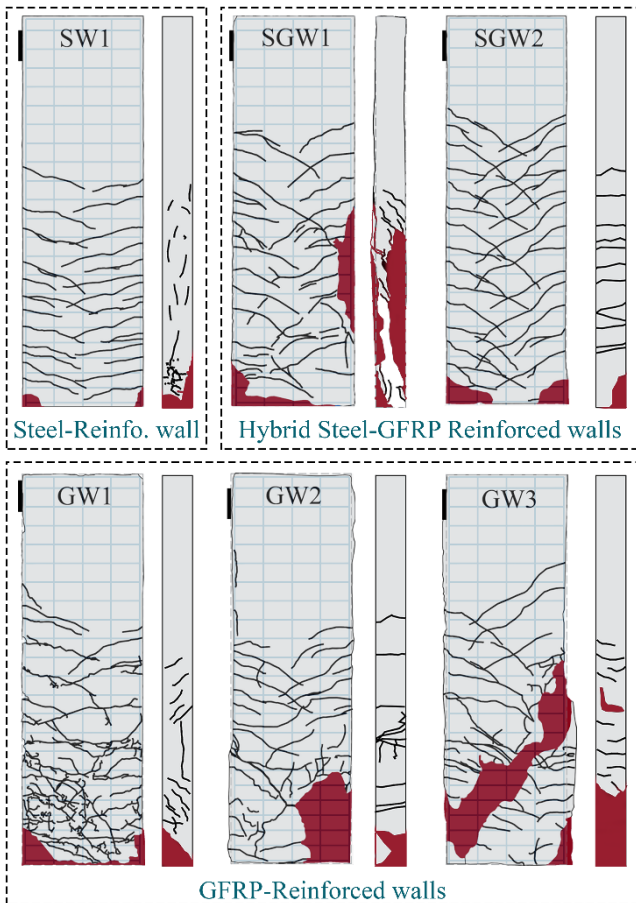


Figure 10 – Observed crack patterns prior to failure

4.2. Self-centering behaviour

The recovered drift ratio over the maximum drift at different levels of drift ratio demands was used to measure the self-centering capabilities of the tested shear walls. Figures 12 and 13 illustrate the residual drift ratio of the steel-reinforced wall (SW1-control wall) during testing. As cyclic loading progressed and higher drift ratios were applied to the walls, they sustained further residual drift ratios in a different value depending on the reinforcement type and ratio.

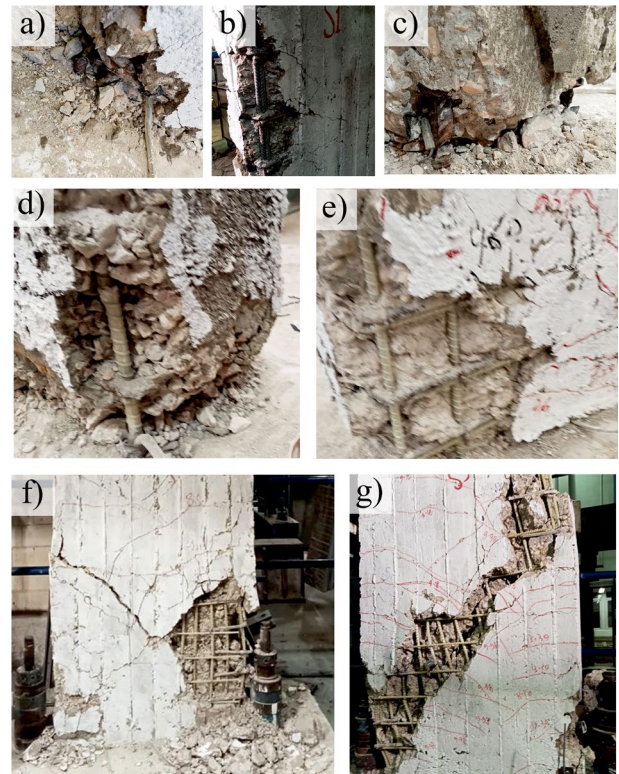


Figure 11 – Close-up photos for the major damage states

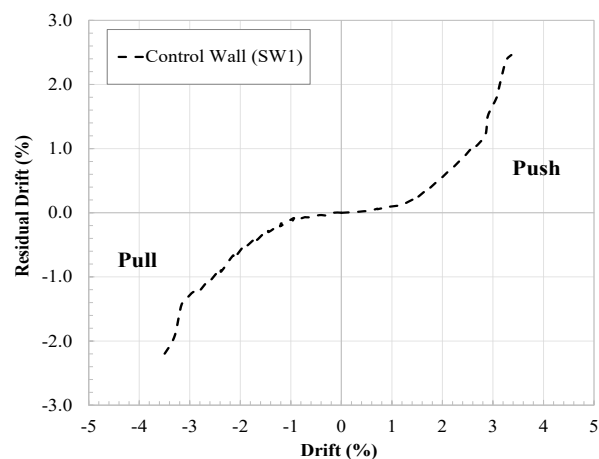


Figure 12 – Residual drift ratio of the steel-reinforced wall (SW1-control wall).

As can be seen in Figures 13a-b, the drift ratio recovery was higher in hybrid steel-GFRP reinforced walls (SGW1 and SGW2) than in control walls. Moreover, GFRP-reinforced walls exhibited smaller residual drifts than their corresponding control walls. Furthermore, the highest drift ratio recoveries occurred in wall GW3, which had the highest GFRP reinforcement ratio. The recovery in the residual drift ratio of each hybrid specimen with respect to the control wall is shown in Figure 13f. According to the obtained results, the maximum self-centering of the slender hybrid wall was observed at 3.6% drift, where the residual drift ratios of the walls SGW1 and SGW2 were 46.5% and 58.3%, respectively, smaller than the steel-reinforced wall. The higher reduction ratio for wall SGW2 compared to wall SGW1 is due to the higher GFRP web reinforcement ratio, see Figure 2. For GFRP-RC walls, maximum reductions in residual drift ratios of 67.1%, 79%, and 80% were attained at 3.6% drift for walls GW1, GW2, and GW3, respectively, compared to the residual drift of the control wall (SW1).

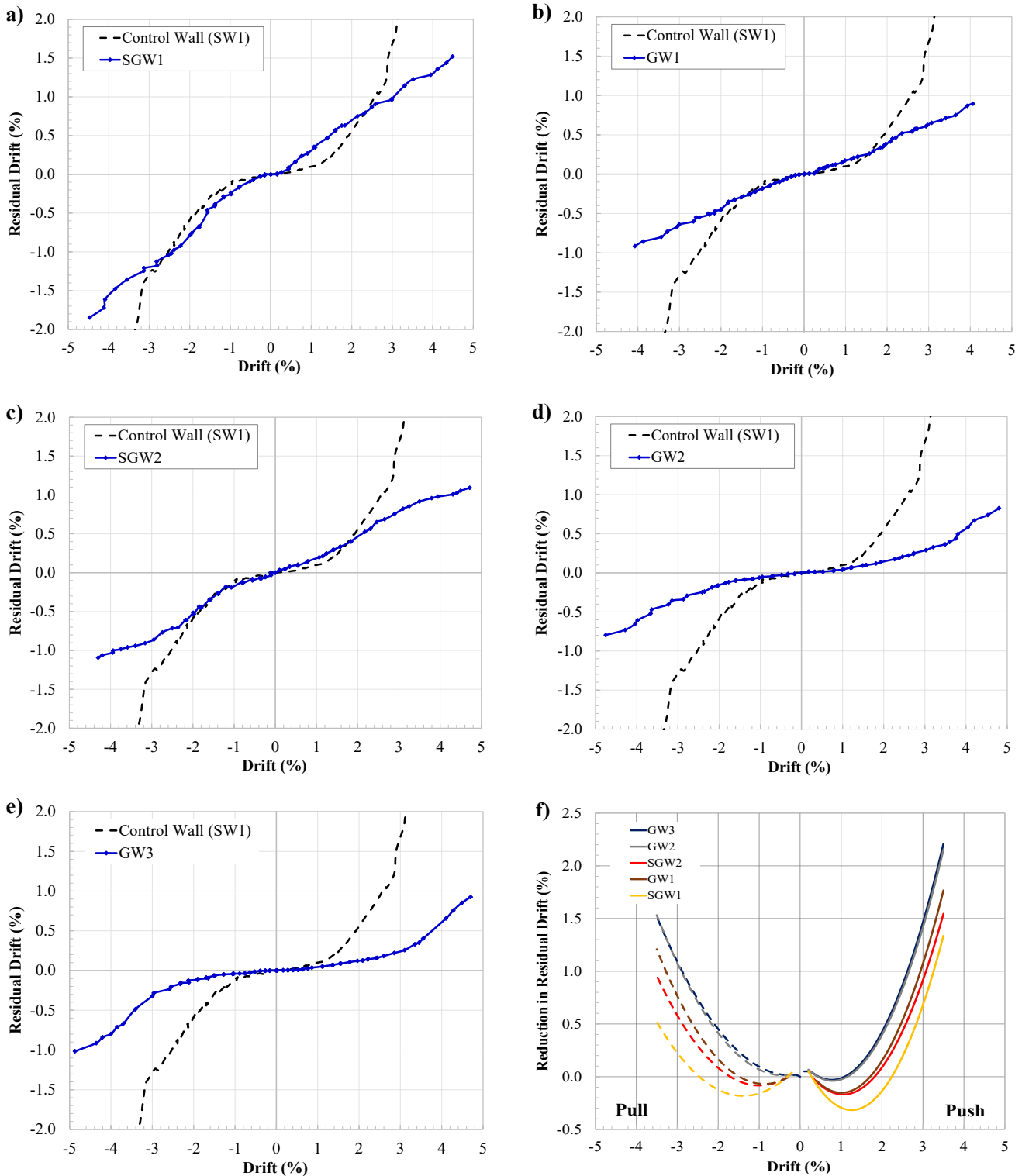


Figure 13 – Residual drift ratio of hybrid steel-GFRP walls (a & b), and GFRP-reinforced walls (c-e), and e) reduction in the residual drift ratios of hybrid walls with respect to control walls.

These results confirm that the minimal recorded residual deformation is due to the capability of self-centering behavior of GFRP-RC walls.

4.3. Energy dissipation and equivalent viscous damping

The dissipated energy during hysteresis (E_d) is given by the area enclosed by the hysteresis loop at each loading increment [31], as shown in Figure 14. The energy dissipated by each successive cycle

was summed up to the energy of the previous cycles to calculate the cumulative energy dissipation. The results showed that lower energy dissipation was calculated for all walls in the early drift levels (lower than 1.0% drift) due to the lower occurred deformation of the tested walls to this drift level. At higher drift levels, steel-reinforced wall (SW1) exhibited the most advantageous energy dissipation capacity (Figure 15). However, the dissipated energy of hybrid steel-GFRP reinforced walls exhibited a similar and considerable increase with the consecutive loading displacement due to the concentrated

vertical steel rebar at the walls' sides. This increase in energy dissipation proved the favorable energy dissipation capacity of the hybrid steel-GFRP reinforced walls. Conversely, due to the elastic behavior of GFRP bars, a lower energy dissipation rate is remarked in GFRP-reinforced walls.

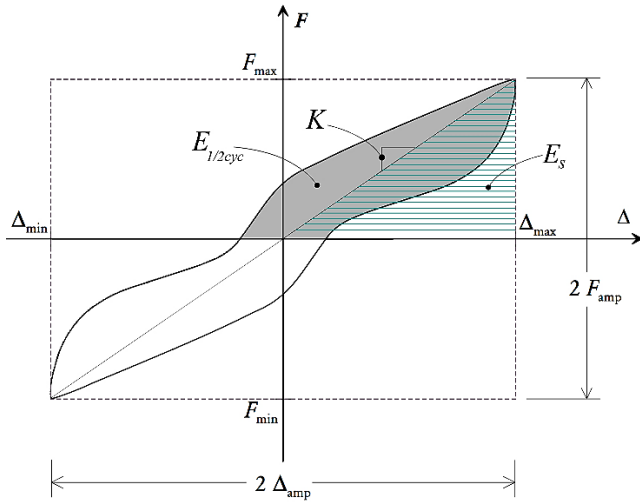


Figure 14 – Calculation of energy dissipation

Additionally, the equivalent viscous damping ratio based on hysteresis, ξ_{hyst} , was used to evaluate the energy dissipation capacity of the shear wall. It was calculated using the area-based method according to the following equation:

$$\xi_{hyst} = \frac{1}{\pi} \frac{E_{1/2cyc}}{F_{amp} \cdot \Delta_{amp}} \quad \text{Eq. 6}$$

where $E_{1/2cyc}$ is the dissipated energy during the half-cycle. $E_s = F_{amp} \cdot \Delta_{amp}$ represents the elastic strain energy of the test wall that is stored in an equivalent linear elastic system in one loading cycle. Figure 16 depicts the relationship between the equivalent viscous damping ξ_{hyst} and the increase in the lateral drift ratios for all tested walls. In general, ξ_{hyst} tends to rise with an increase in drift ratio.

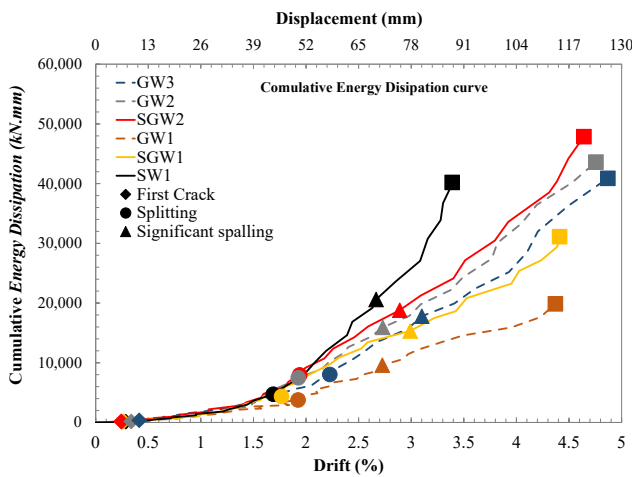


Figure 15 – Evolution of energy dissipation of tested walls

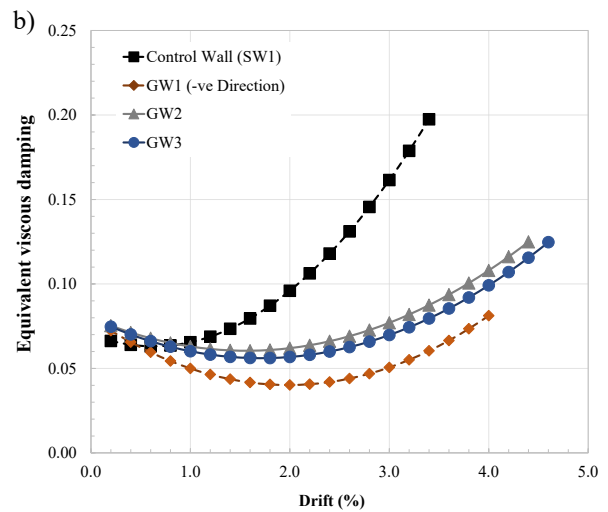
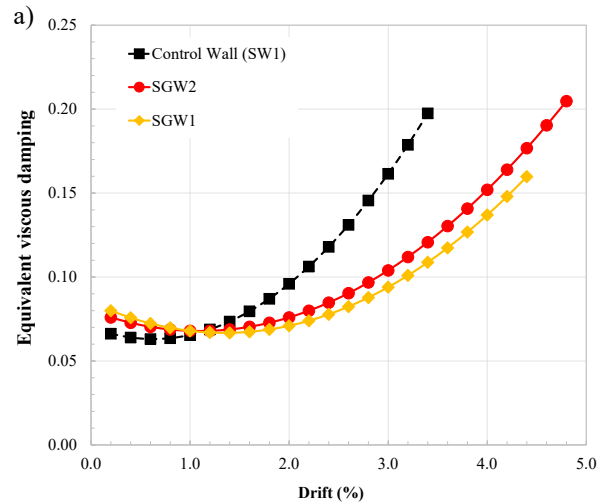


Figure 16 – Equivalent viscous damping coefficient: comparison between control steel-reinforced wall and a) hybrid steel-GFRP reinforced walls, b) GFRP-reinforced walls

Moreover, the obtained results showed that the steel-reinforced and hybrid steel-GFRP reinforced walls exhibited higher significantly equivalent viscous damping ratios compared to the GFRP-reinforced walls because of the plastic deformation of deformed steel bars. The equivalent viscous damping ratio reached 11.7% and 14.1% at the ultimate load and achieved 16.1% to 20.5% at the displacement of $2\Delta_u$ for hybrid steel-GFRP reinforced walls SGW1 and SGW2, respectively. By contrast, the GFRP-RC walls exhibited approximately 59%, 36%, and 35.8% reduction of ξ_{hyst} at ultimate load than that of the control steel-reinforced wall (SW1).

4.4. Damage indices

Various damage indices were proposed in the literature [32-36], among others, in order to measure the resultant deficiencies and vulnerability of the structural members under seismic loading. Recently, various applications of damage indices were achieved based on loading history demand and capacity for estimating the damage and repair costs. Moreover, they are also utilized for decision-making in the post-earthquake evaluation and safety or vulnerability assessment for existing structures. Also, the performance levels of structural members can be evaluated at different drift levels using damage indices [37]. In general, the damage states were classified into the following five levels [35]:

$DI < 0.10$ No damage or minor local cracks

$0.10 \leq DI < 0.25$	Minor damage (e.g., light cracking throughout)
$0.25 \leq DI < 0.40$	Moderate damage (e.g., severe cracking local spalling)
$0.40 \leq DI < 1.0$	Sever damage (e.g., Concrete crushing and expose of bars)
$DI \geq 1.0$	Collapse

Following the approach found in the literature [30, 37], various damage indices for the tested walls were calculated to investigate the damage propagation and failure rate of all tested walls.

Moreover, the resultant damage status in the hybrid steel-GFRP reinforced walls and GFRP-RC walls were compared with the control steel-reinforced wall (SW1). Table 2 includes the formulation of adopted damage indices. Figure 17 depicts the damage indices based on displacement, dissipated energies, and effective stiffness, as well as the combined and performance indices, which were also plotted for all tested walls.

According to the results obtained from the damage index, based on the dissipated energy, the steel-reinforced wall (SW1) had lower damage than GFRP-reinforced walls at the early drift levels.

However, a considerably higher damage rate was observed at the drift level corresponding to the yielding of steel bars. On the other hand, by analyzing the damage indices based on displacement energy and

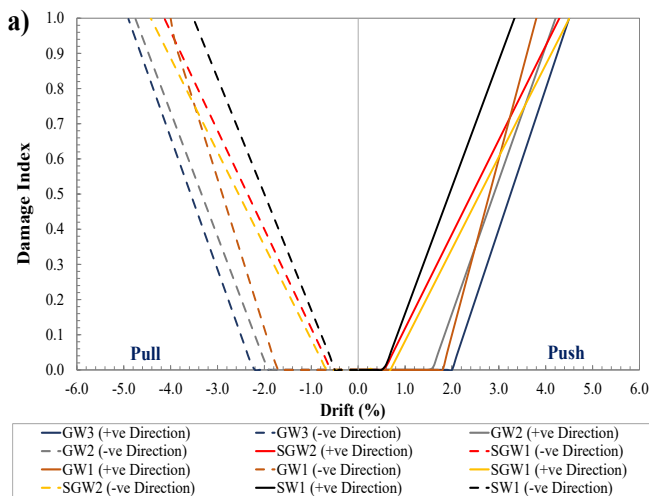
stiffness, the GFRP-RC walls experienced lower damage when compared with the steel-reinforced wall (SW1) at the same drift level as a result of its softer response with extensive concrete damage. Furthermore, the combined damage index also showed a more significant drift level of hybrid steel-GFRP, and GFRP reinforced walls with equal damage index compared to the control wall (SW1). This response of walls SGW1, SGW2, and walls GW1, GW2, and GW3 is mainly due to the low modulus of elasticity of GFRP bars, which allowed the walls to sustain higher deformation, at advanced loading levels, till failure. Moreover, by analyzing the performance index (Figure 17e), hybrid steel-GFRP and GFRP reinforced walls showed similar damage propagation where a lower damage rate was attained when compared with steel-reinforced wall at the same drift level.

5. Summary and conclusions

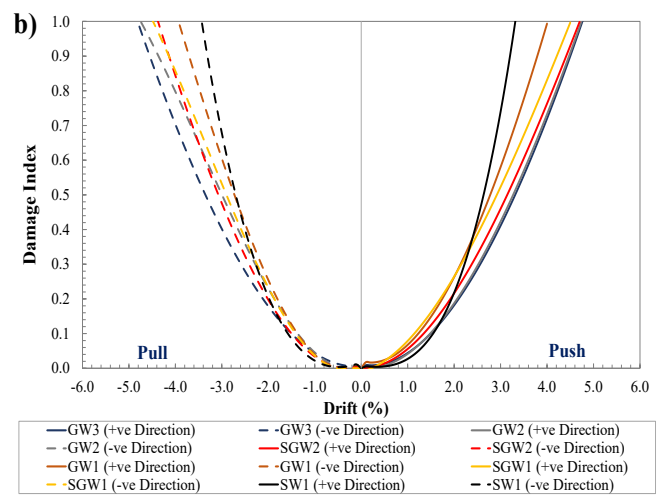
The current study was conducted on RC concrete shear walls to investigate the effectiveness of a hybrid steel-GFRP system in reinforcing shear walls to withstand seismic loads. To accurately study the impact of the GFRP reinforcement ratio on the overall behavior and self-centering performance of RC shear walls, several reinforcement ratios were selected for the hybrid steel-GFRP reinforced walls and the GFRP-reinforced walls. The results are encouraging for applying hybrid steel-GFRP reinforcement since the walls reached their maximum strength without exhibiting any signs of sliding shear failure, instability, or anchorage failure.

Table 2 - Different damage indices proposed by the researchers, [30,37]

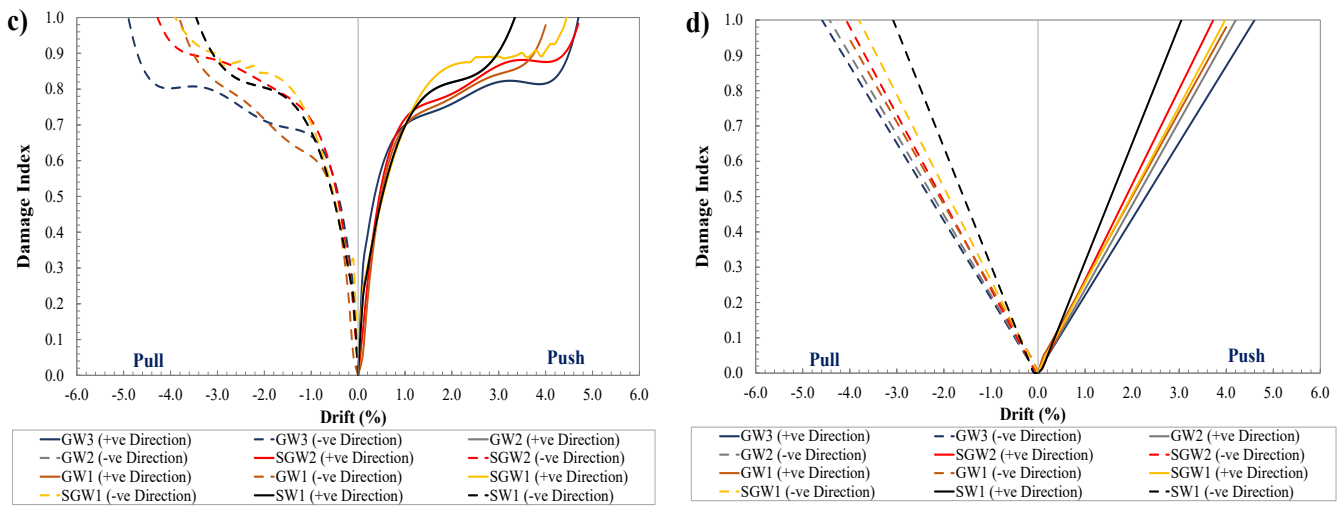
Damage index	Type	Formulation	Parameter Values
Powell & Allahabadi [25]	Based on the displacement	$DI = \frac{\Delta_m - \Delta_y (or \Delta_e)}{\Delta_u - \Delta_y (or \Delta_e)}$ $DI = \frac{\mu_m - 1}{\mu_u - 1}$	$\mu_u = \frac{\Delta_u}{\Delta_y (or \Delta_e)}$ $\mu_m = \frac{\Delta_m}{\Delta_y (or \Delta_e)}$
Rodriguez and Padilla [26]	Based on dissipated energy	$DI = \sum_{i=0}^n \frac{\int dE}{E}$	$E =$ Energy dissipation
Kunnath & Jenne [27]	Based on effective Stiffness	$DI = 1 - \frac{K_m}{K_i}$	$K_m =$ Secant stiffness $K_i =$ Initial stiffness $\beta = 0.25$
Park and Ang [28]	Combined index	$DI = \frac{\Delta_m}{\Delta_u} + \beta \frac{\int dE}{F_y (or e) \Delta_u}$	$F_y (or e) =$ Load at yielding for steel bars or spalling concrete for GFRP bars
Promis and Ferrier [29]	Performance index	$P = \frac{\sum E_m D_m}{\sum E_m}$	$E_m =$ Dissipated energy $D_m =$ Combined index in function of ductility and dissipated energy



Linear damage index proposed by Powell and Allahabadi [32]

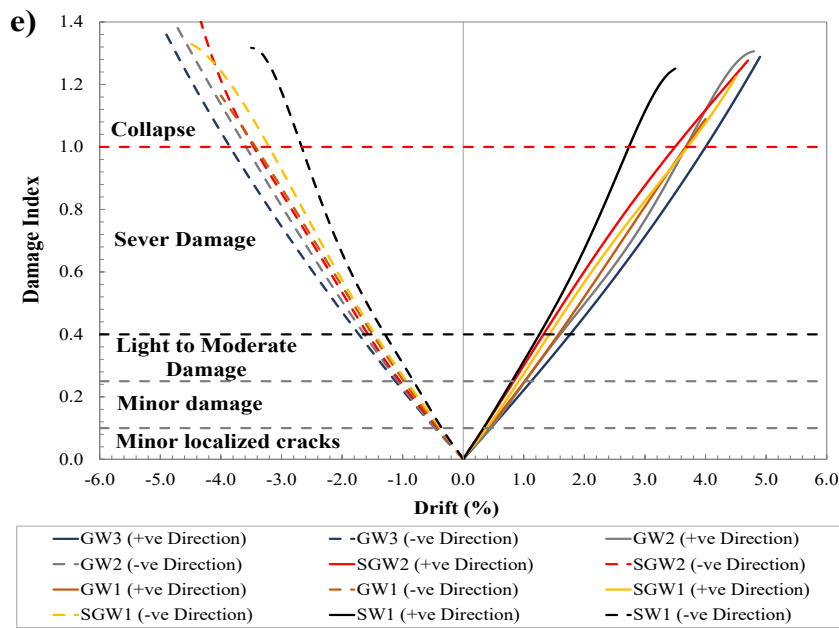


Damage index based on energy proposed by [33]



Damage index based on stiffness proposed by [34]

Combined damage index proposed by [35]



Performance index proposed by [36]

Figure 17 –Damaged indices of tested walls

The findings confirmed that the permeant/plastic deformations in the concrete are the source of the cumulative energy dissipation in GFRP-reinforced shear walls. Due to the elasticity of the GFRP reinforcement, all GFRP-reinforced walls exhibited relatively similar levels of energy dissipation at the same loading step. Moreover, GFRP-RC walls showed stable hysteretic performance with a higher drift capacity than steel-reinforced walls. Furthermore, increasing the GFRP-reinforcement ratio enhances the ultimate load capacity and significantly reduces crack width at moderate damage levels.

In addition, for hybrid steel-GFRP and GFRP-reinforced walls compared to the steel-reinforced wall, the elastic behavior of GFRP bars led to lower damage rates with realigned cracks and recoverable deformation at the same drift level. At higher drift levels, a remarkably similar failure pattern of steel-reinforced and hybrid steel-GFRP-RC walls was attained that was characterized by local buckling of the outmost longitudinal steel bars and crushing of concrete at the toe of the walls. The most significant advantage of using hybrid steel-GFRP reinforcement in shear walls is having a higher self-centering capacity for the walls. It mitigates the post-yield strength deterioration observed in conventional steel-reinforced walls. Almost similar strength, stiffness, and drift capacity were

achieved for hybrid steel-GFRP reinforcement compared to the walls of conventional steel reinforcement. However, a reduction of 11.7% to 14.1% in the equivalent viscous damping ratio was calculated for hybrid steel-GFRP reinforced walls when replacing the web steel reinforcement, depending on the GFRP-reinforcement ratio. Since the hybrid GFRP-steel reinforcement scheme is an appropriate alternative for RC shear walls, additional investigation is needed to address other aspects and develop design guidelines for practical application.

Nomenclature

- GFRP Glass-Fiber-Reinforced Polymer
- LVDT Linear variable differential transformers
- RC Reinforced Concrete
- SW Shear wall
- a* depth of equivalent rectangular stress block
- A_b* Cross-sectional area of an individual reinforcement bar
- A_c* area of concrete section
- A_f* area of GFRP reinforcement

A_{fv}	amount of FRP shear reinforcement within spacing s
A_s	area of reinforcement bars
b_w	Thickness of the wall web
c	distance from extreme compression fibre to neutral axis
c'	clear cover of reinforcement
d	distance from extreme compression fibre to centroid of longitudinal tension reinforcement
E_c	modulus of elasticity of concrete
E_d	energy dissipation through hysteretic damping
E_s	elastic dissipated energy
E_f	guaranteed modulus of elasticity of GFRP
E_s	modulus of elasticity of steel reinforcement
f'_c	specified compressive strength of concrete
f_s	stress in reinforcement bars
f_u	specified tensile strength of steel reinforcement,
f_y	specified yield strength for steel reinforcement
f_{fv}	tensile strength of FRP for shear design
h_w	height of entire wall from base to top
k	ratio of depth of neutral axis to reinforcement depth
l_w	length of entire wall
M_i	sum of moments around the centroid
n_f	ratio of modulus of elasticity of FRP bars to modulus of elasticity of concrete
P_i	theoretical external applied axial load
s	Spacing between two successive stirrups is the distance from the vertical reinforcement at point n to the end of the compression toe
X_i	aspect ratio
α_s	target top-displacement of the tested walls
Δ	displacement at the maximum capacity
Δ_u	yield displacement
Δ_y	top-drift of the tested walls
δ	load multiplier ($\lambda = \frac{q}{w_w}$)
ε_c	strain in concrete
ε_{cu}	ultimate strain in concrete
ε_{si}	strain in reinforcement bars
$\rho_{v,s}$	ratio of steel reinforcement in the vertical direction
$\rho_{h,s}$	ratio of steel reinforcement in the horizontal direction
$\rho_{v,f}$	ratio of GFRP reinforcement in the vertical direction
$\rho_{h,f}$	ratio of GFRP reinforcement in the horizontal direction

Declaration of Conflict of Interests

The authors declare that there is no conflict of interest. They have no known competing financial interests or personal relationships that could have appeared to influence the work reported in this paper.

References

- [1.] Z. Tuna, Seismic Performance, Modeling, and Failure Assessment of Reinforced Concrete Shear Wall Buildings, Los Angeles: PhD Thesis, University of California, 2012.
- [2.] K. Beyer, A. Dazio ve M. J. N. Priestley, «Quasi-Static Cyclic Tests of Two U-Shaped Reinforced Concrete Walls,» *Journal of Earthquake Engineering*, cilt 12, no. 7, pp. 1023-1053, 2008.
- [3.] F. Talaei, Numerical Simulation and Economic Design of Concrete Shear Walls Reinforced with GFRP Bars, Alberta, Canada: M.Sc. Thesis, University of Alberta, 2017.
- [4.] K. Orakcal, L. M. Massone ve J. W. Wallace, «Shear Strength of Lightly Reinforced Wall Piers and Spandrels,» *ACI Structural Journal*, cilt 106, no. 4, pp. 455-465, 2009.
- [5.] Y.-H. Oh, S. W. Han ve L.-H. Lee, «Effect of boundary element details on the seismic deformation capacity of structural walls,» *Earthquake Engineering and Structural Dynamics*, cilt 31, no. 8, pp. 1583-1602, 2002.
- [6.] M. Preti ve E. Giuriani, «Ductility of a Structural Wall with Spread Rebars Tested in Full Scale,» *Journal of Earthquake Engineering*, cilt 15, no. 8, pp. 1238-1259, 2011.
- [7.] L. M. Massone, K. Orakcal ve J. W. Wallace, «Flexural and shear responses in slender RC shear walls,» %1 içinde 13th World Conference on Earthquake Engineering, Vancouver, B.C., Canada, 2004.
- [8.] C. Kassem, A. S. Farghaly ve B. Benmokrane, «Evaluation of Flexural Behavior and Serviceability Performance of Concrete Beams Reinforced with FRP Bars,» *Journal of Composites for Construction*, cilt 15, no. 5, pp. 682-695, 2011.
- [9.] C. E. Bakis, L. C. Bank, V. L. Brown, E. Cosenza, J. F. Davalos, J. J. Lesko, A. Machida, S. H. Rizkalla ve T. C. Triantafyllou, «Fiber-Reinforced Polymer Composites for Construction—State-of-the-Art Review,» *Journal of Composites for Construction*, cilt 6, no. 2, pp. 73-87, 2002.
- [10.] E. El-Salakawy, B. Benmokrane, A. El-Ragaby ve D. Nadeau, «Field Investigation on the First Bridge Deck Slab Reinforced with Glass FRP Bars Constructed in Canada,» *Journal of Composites for Construction*, cilt 9, no. 6, pp. 470-479, 2005.
- [11.] M. K. Sharbatdar ve M. Saatcioglu, «Seismic Design of FRP Reinforced Concrete Structures,» *Asian Journal of Applied Sciences*, cilt 2, no. 3, pp. 211-222, 2009.
- [12.] H. Tobbi, A. S. Farghaly ve B. Benmokrane, «Concrete Columns Reinforced Longitudinally and Transversally with Glass Fiber-Reinforced Polymer Bars,» *ACI Structural Journal*, cilt 109, no. 4, pp. 551-558, 2012.
- [13.] N. Mohamed, A. S. Farghaly, B. Benmokrane ve K. W. Neale, «Flexure and Shear Deformation of GFRP-Reinforced Shear Walls,» *Journal of Composites for Construction*, cilt 18, no. 2, p. 04013044, 2014.
- [14.] M. R. Ehsani, «Glass-fiber reinforcing bars,» %1 içinde Alternative Materials for the Reinforcement and Prestressing of Concrete, J. L. Clarke, Dü., New York, NY, E & FN & SPON, CRC Press, 1993, pp. 34-54.
- [15.] A. Nanni, «Flexural Behavior and Design of RC Members Using FRP Reinforcement,» *Journal of Structural Engineering*, cilt 119, no. 11, pp. 3344-3359, 1993.
- [16.] T. Yamakawa ve T. Fujisaki, «A study on elasto-plastic behavior of structural walls reinforced by CFRP grids,» %1 içinde Non-Metallic (FRP) Reinforcement for Concrete Structures, L. Taerwe, Dü., London, CRC Press, 1995, p. 306-313.
- [17.] N. Mohamed, A. S. Farghaly, B. Benmokrane ve K. W. Neale, «Experimental Investigation of Concrete Shear Walls Reinforced with Glass Fiber-Reinforced Bars under Lateral Cyclic Loading,» *Journal of Composites for Construction*, cilt 18, no. 3, pp. A4014001-1-12, 2014.
- [18.] A. Arafa, A. S. Farghaly ve B. Benmokrane, «Experimental Behavior of GFRP-Reinforced Concrete Squat Walls Subjected to Simulated Earthquake Load,» *Journal of Composites for Construction*, cilt 22, no. 2, pp. 04018003-1-14, 2018.
- [19.] M. Z. Afifi, H. M. Mohamed, O. Chaallal ve B. Benmokrane, «Confinement Model for Concrete Columns Internally Confined with Carbon FRP Spirals and Hoops,» *Journal of Structural Engineering*, cilt 141, no. 9, p. 04014219, 2015.
- [20.] Q. Zhang, J. Xiao, Q. Liao ve Z. Duan, «Structural behavior of seawater sea-sand concrete shear wall reinforced with GFRP bars,» *Engineering Structures*, cilt 189, pp. 458-470, 2019.
- [21.] I. Shabana, A. S. Farghaly ve B. Benmokrane, «Effect of Axial Load and Web Reinforcement Ratio on Seismic Behavior of Glass Fiber-Reinforced Polymer-Reinforced Concrete Squat Walls,» *ACI Structural Journal*, cilt 118, no. 4, pp. 109-121, 2021.
- [22.] ACI 318, Building code requirements for structural concrete and Commentary (ACI 318-19), Farmington Hills, MI: American Concrete Institute, 2019.
- [23.] ACI 440.1R, Guide for the design and construction of structural concrete reinforced with FRP bars, Farmington Hills, MI: American Concrete Institute, 2015.

- [24.] A. Hassanein, N. Mohamed, A. S. Farghaly ve B. Benmokrane, «Effect of boundary element confinement configuration on the performance of GFRP-Reinforced concrete shear walls,» *Engineering Structures*, cilt 225 , p. 111262, 2020.
- [25.] ACI 440.1R-15, Guide for the design and construction of structural concrete reinforced with FRP bars, Farmington Hills, MI: American Concrete Institute, 2015.
- [26.] T. Paulay ve M. J. N. Priestley, *Seismic design of reinforced concrete and masonry buildings*, New York.: John Wiley and Sons Inc., 1995.
- [27.] O. A. El-Azizy, M. T. Shedid, W. W. El-Dakhkhni ve R. G. Drysdale, «Experimental evaluation of the seismic performance of reinforced concrete structural walls with different end configurations,» *Engineering Structures*, cilt 101, p. 246–263, 2015.
- [28.] ASTM C39/C39M, «Standard test method for compressive strength of cylindrical concrete specimens,» American Society for Testing and Materials, West Conshohocken, PA, 2021.
- [29.] FEMA 461, «Interim Testing Protocols for Determining the Seismic Performance Characteristics of Structural and Nonstructural Components,» Federal Emergency Management Agency, Redwood, CA , 2007.
- [30.] S. M. Hosseini, M. Yekrangnia ve A. V. Oskouei, «Effect of spiral transverse bars on structural behavior of concrete shear walls reinforced with GFRP bars,» *Journal of Building Engineering*, cilt 55, p. 104706, 2022.
- [31.] A. K. Chopra, *Dynamics of structures: Theory and applications to earthquake engineering*, Englewood Cliffs, NJ: Prentice-Hall, Inc., 2000.
- [32.] G. H. Powell ve R. Allahabadi, «Seismic damage prediction by deterministic methods: concepts and procedures,» *Earthquake Engineering and Structural Dynamics*, cilt 16, no. 5, pp. 719-734, 1988.
- [33.] M. E. Rodriguez ve D. Padilla, «A damage index for the seismic analysis of reinforced concrete members,» *Journal of Earthquake Engineering*, cilt 13, no. 3, pp. 364-383, 2009.
- [34.] S. K. Kunnath ve C. Jenne, «Seismic damage assessment of inelastic RC structures,» %1 içinde 5th US national conference on earthquake engineering, EERI Chicago, Illinois, 1994.
- [35.] Y.-J. Park, A. H.-S. Ang ve Y. K. Wen, «Seismic damage analysis of reinforced concrete buildings,» *Journal of Structural Engineering*, cilt 111, no. 4, pp. 740-757, 1985.
- [36.] G. Promis ve E. Ferrier, «Performance indices to assess the efficiency of external FRP retrofitting of reinforced concrete short columns for seismic strengthening,» *Construction and Building Materials*, cilt 26, pp. 32-40, 2012.
- [37.] M. Haji, H. Naderpour ve A. Kheyroddin, «Experimental study on influence of proposed FRP-strengthening techniques on RC circular short columns considering different types of damage index,» *Composite Structures*, cilt 209, pp. 112-128, 2019.

How to Cite This Article

el-Kady, H., Amer, O., Ali, A., and Haggag, H., Seismic Performance Assessment of Hybrid GFRP-Steel reinforced concrete Shear Walls, *Civil Engineering Beyond Limits*, 3 (2022), 1737.
<https://doi.org/10.36937/cebel.2022.1737>